Supporting Information

Magneto-structural correlation of cyano-substituted 3-*tert*-butyl-1-phenyl-1,2,4-benzotriazin-4-yl: spin transition behaviour observed in a 6-cyano derivative

Yusuke Takahashi, Naoya Tsuchiya, Youhei Miura and Naoki Yoshioka*

Department of Applied Chemistry, Faculty of Science and Technology, Keio University, Yokohama 223-8522, Japan.
E-mail: yoshioka@applc.keio.ac.jp

Table of Contents

Magnetic Properties

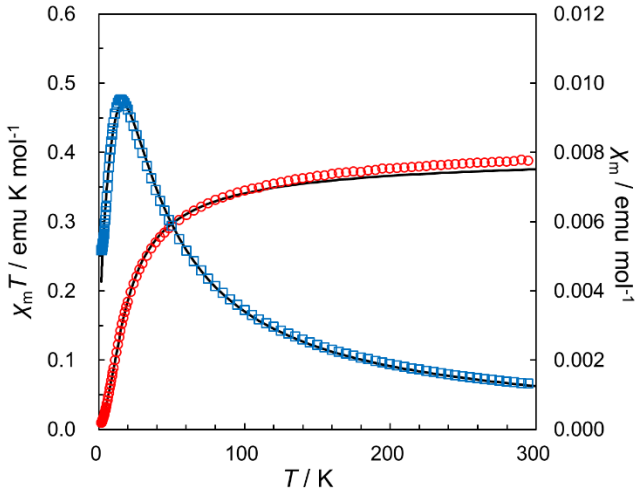

Fig. S1 Thermal dependence of $\chi_m T$ and χ_m for **7CN**. The solid lines represent the best-fit result of the 1D antiferromagnetic chain model (correlation factor $R = \Sigma[\chi_{m\ obs}-\chi_{m\ calcd}]^2/\Sigma[\chi_{m\ obs}]^2 = 5.25 \times 10^{-4}$).

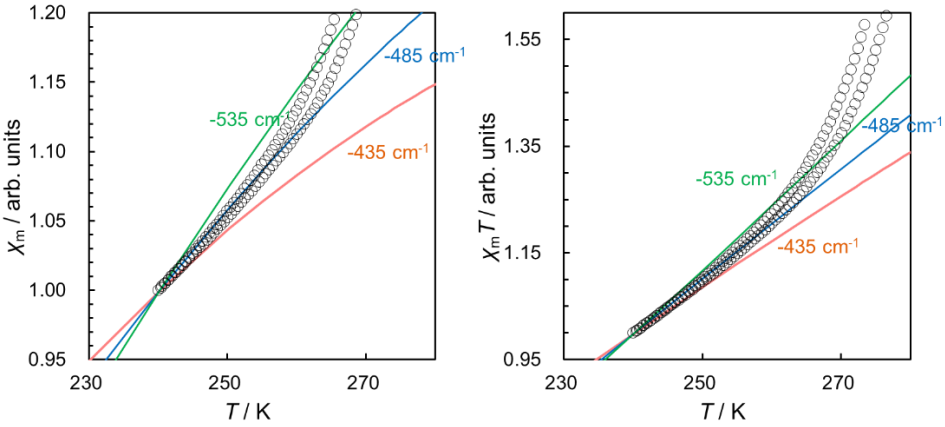

Fig. S2 Temperature dependence of normalized χ_m and $\chi_m T$ of LT phase of Al foil wrapped sample of **6CN** for the rough estimation of the magnitude of the intermolecular magnetic interaction using the Bleaney-Bowers model. The experimental and theoretical values of χ_m and $\chi_m T$ were normalized by the corresponding value of 240 K.

Crystallographic Data

Table S1 Crystallographic data of **7CN** and **6CN**.

	7CN	**6CN** (HT)	**6CN** (LT)[a]
Chemical formula	$C_{18}H_{17}N_4$	$C_{18}H_{17}N_4$	$C_{18}H_{17}N_4$
Formula weight	289.36	289.36	289.36
Temperature / K	296	300	263
Crystal size / mm^3	0.74 × 0.17 × 0.08	1.24 × 0.54 × 0.06	1.24 × 0.54 × 0.06
Space group	*I*2/*a* (No. 15)	*I*2/*a* (No. 15)	*P*-1 (No. 2)
a / Å	18.709(3)	26.317(4)	6.8527(6)
b / Å	7.8316(12)	6.7524(7)	9.1813(9)
c / Å	21.501(6)	18.003(2)	13.1091(12)
α / °	90	90	86.834(3)
β / °	90.945(4)	90.578(3)	80.616(3)
γ / °	90	90	74.983(3)
V / $Å^3$	3149.9(11)	3199.0(7)	785.88(13)
Z	8	8	2
d_{calc} / g cm^{-3}	1.220	1.202	1.223
μ / mm^{-1}	0.075	0.074	0.075
F(000)	1224	1224	306
θ (min, max) / °	2.18, 23.02	2.73, 24.44	2.77. 25.10
Index ranges	$-19 \le h \le 20$ $-8 \le k \le 8$ $-23 \le l \le 22$	$-30 \le h \le 30$ $-7 \le k \le 7$ $-18 \le l \le 20$	$-7 \le h \le 8$ $-10 \le k \le 10$ $0 \le l \le 15$
Measured reflection	10772	13670	2512
Independent reflection (R_{int})	2196 (0.0486)	2605 (0.0641)	2512 (-)
Observed reflection ($I \ge 2\sigma(I)$)	1422	1929	1707
Goodness of fit on F^2	1.380	1.396	1.103
R, R_w ($I \ge 2\sigma(I)$)	0.0702, 0.1891	0.0712, 0.2160	0.0647, 0.1763
R, R_w (all data)	0.1153, 0.2190	0.0901, 0.2370	0.0975, 0.2128
Resd density (min, max) / *e* $Å^{-3}$	-0.300, 0.438	-0.190, 0.289	-0.276, 0.220

[a] The data of LT phase for **6CN** was obtained as twinning crystal and it was analyzed using *TWINABS* program.

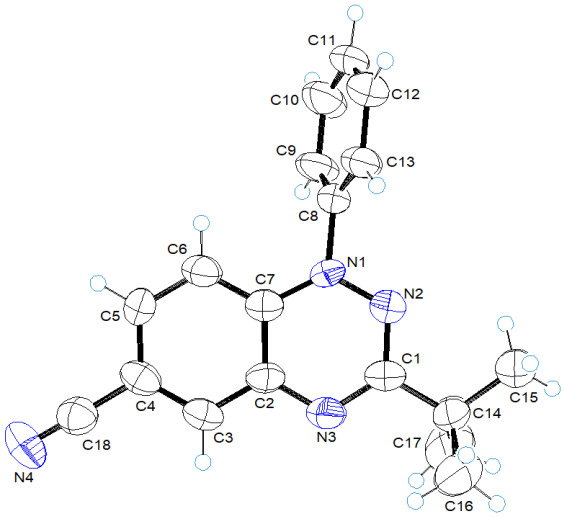

Fig. S3 ORTEP drawing of LT phase of **6CN** (50% thermal ellipsoids).

Table S2 Selected bond lengths and dihedral angle of benzotriazinyl radicals.

Compound		$d_{N1–N2}$ / Å	$d_{N2–C1}$ / Å	$d_{C1–N3}$ / Å	dihedral angle / °
7CN		1.375(3)	1.324(4)	1.335(4)	45.236(80)
6CN	HT	1.360(3)	1.330(3)	1.332(3)	68.408(97)
	LT	1.364(3)	1.325(4)	1.339(4)	69.858(130)

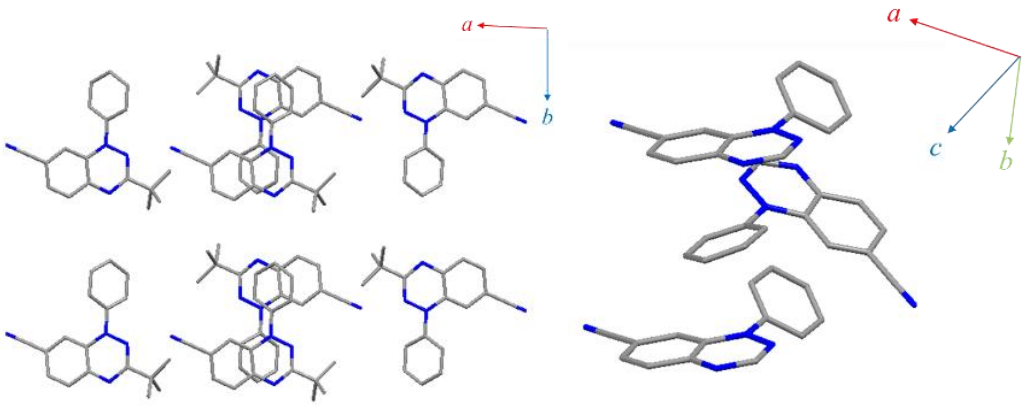

Fig. S4 Molecular arrangement of **7CN**. The selected *tert*-butyl groups were omitted for clarity.

Table S3 The longitudinal and latitudinal slippages of **6CN**.

Pair	T / K(phase)	ϕ_1 / °	ϕ_2 / °
I-II	300 (HT)	50.8	66.0
	263 (LT)	57.2	65.2
II-I’	300 (HT)	47.2	64.5
	263 (LT)	43.2	67.1

Computational Data

Table S4 The calculation result of the intermolecular interaction for **7CN** at UB3LYP and UBLYP level, and 6-31G(d) basis set. BS and T represent broken symmetry singlet and triplet state.

Pair	Function	Spin state	Energy / a.u.	$<S^2>$	J / cm^{-1}
Pair A	UB3LYP	BS	-1829.6052263	1.027120	-3.4
		T	-1829.6052110	2.027955	
	UBLYP	BS	-1828.7856173	1.003589	-8.7
		T	-1828.7855779	2.008456	
Pair B	UB3LYP	BS	-1829.6155189	1.027472	+0.2
		T	-1829.6155196	2.027491	
	UBLYP	BS	-1828.7979382	1.008204	-0.04
		T	-1828.7979380	2.008332	
Pair C	UB3LYP	BS	-1829.6079463	1.027894	-0.04
		T	-1829.6079461	2.027898	
	UBLYP	BS	-1828.7908988	1.008365	-0.11
		T	-1828.7908983	2.008430	

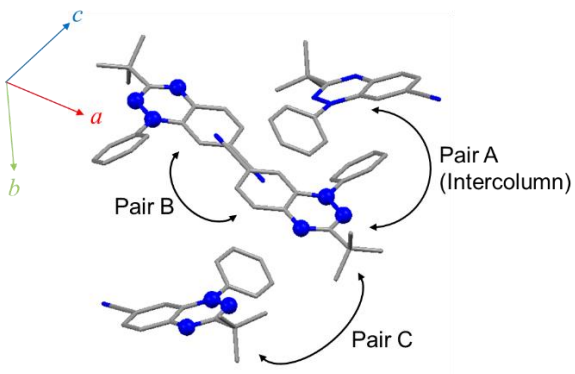

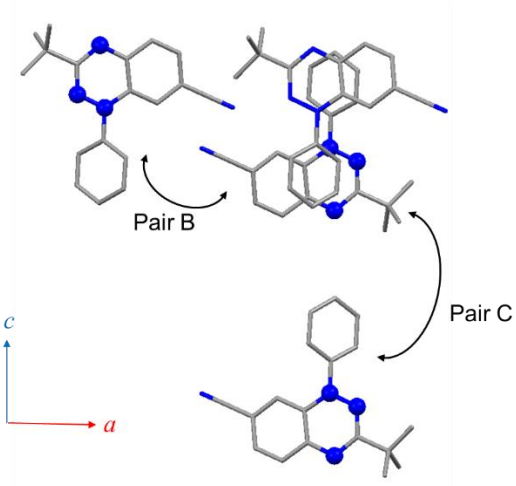

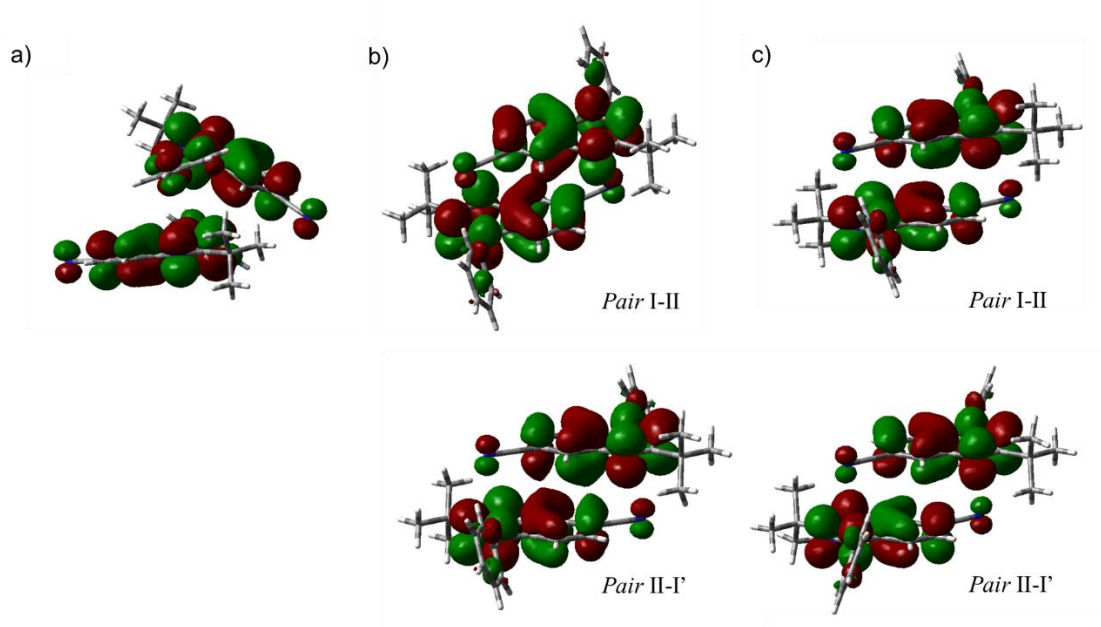

Fig. S5 Overlap of SOMOs for (a) **7CN**, (b) **6CN**(HT) and (c) **6CN**(LT).

Table S5 The calculation results of **6CN** at UB3LYP/6-31G(d) level. BS and T represent broken symmetry singlet and triplet state.

Pair (Phase)	Spin state	Energy / a.u.	$\langle S^2 \rangle$	$2J$ / cm^{-1}
I-II(HT)	BS	-1829.5998682	1.025442	+4.5
	T	-1829.5998784	2.027256	
I-II(LT)	BS	-1829.6097942	0.980403	-587.5
	T	-1829.6085162	2.027684	
II-I'(HT)	BS	-1829.5974589	1.026153	+10.9
	T	-1829.5974837	2.027356	
II-I'(LT)	BS	-1829.6107765	1.025442	-147.5
	T	-1829.6104445	2.027256	

EPR Data

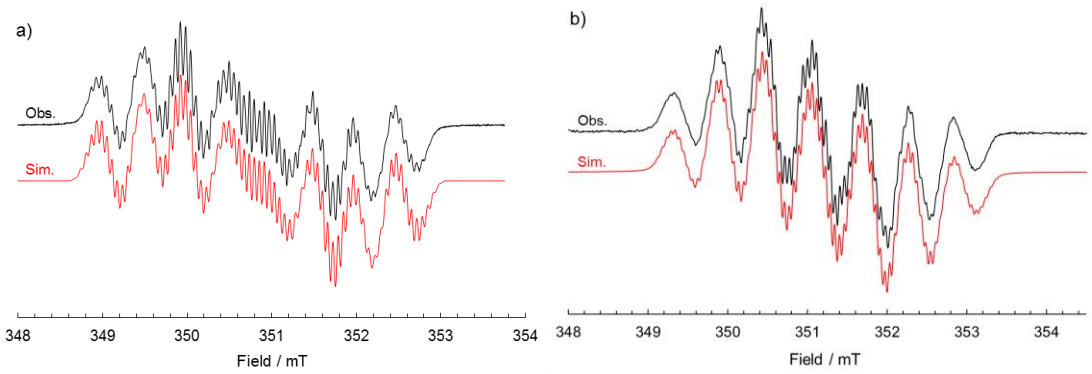

Fig. S6 EPR spectra of (a) **7CN** and (b) **6CN** in toluene at room temperature; black and red lines denote the observed and simulated spectra, respectively.

Table S6 The hfccs and *g*-factor of **7CN** and **6CN**.

	hfcc / mT	
nuclei	**7CN**	**6CN**
N1	0.752	0.687
N2	0.462	0.516
N3	0.495	0.517
CN	0.113	0.800
H3	0.125	0.120
H4	0.117	-
H5	-	0.169
H6	0.113	0.101
H9,13	0.061	0.066
H10, 12	0.060	0.053
H11	0.061	0.048
g-factor	2.0039	2.0040

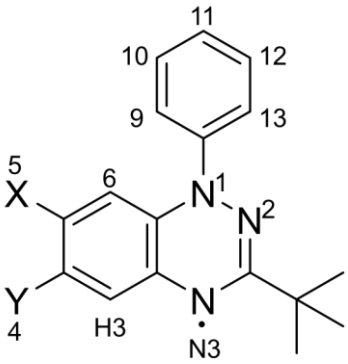

7CN: X = CN, Y = H
6CN: X = H, Y = CN

UV-Vis Spectra

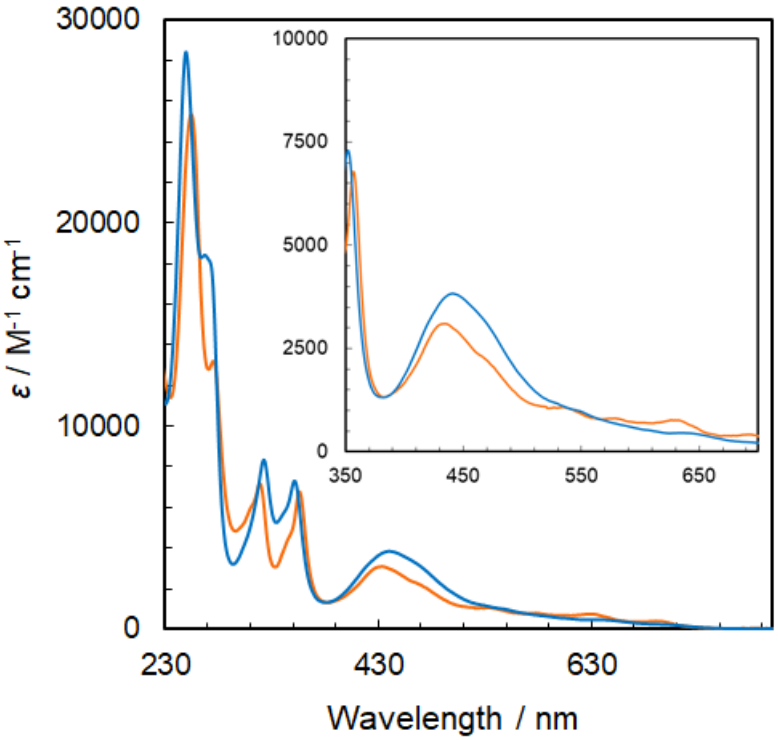

Fig. S7 UV-Vis spectra of **7CN**(blue) and **6CN**(orange) in CH_2Cl_2.

Table S7 The wavelength of maximum absorption (λ_{max}) of **7CN** and **6CN**.

Compound	λ_{max} (molar absorbance coefficient, ε /10^3 M^{-1} cm^{-1})
7CN	250(28.4), 263(18.4), 323(8.33), 352(7.30), 441(3.82)
6CN	255(25.4), 276(13.2), 319(7.17), 356(6.78), 435(3.10), 632(0.764)

Cyclic Voltammograms

The cyclic voltammograms of 7CN and 6CN are shown in Figure S8. Two reversible waves corresponding to the reduction and oxidation processes were observed.

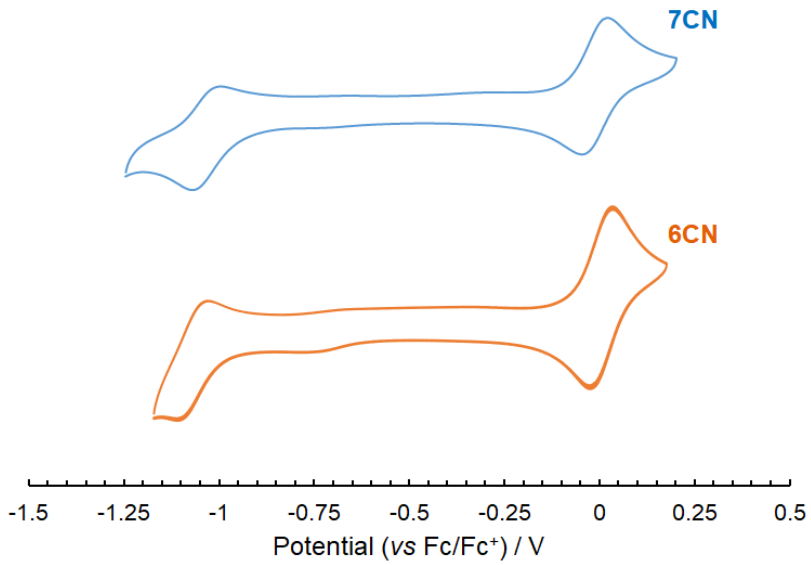

Figure S8. Cyclic voltammograms of **7CN** and **6CN** in CH_3CN containing 0.1 M tetrabutylammonium hexafluorophosphate as the supporting electrolyte.

Table S8 The redox potential of **7CN** and **6CN**.

Compound	Potential (vs. Fc/Fc^+)	
	E_1	E_2
7CN	-1.03	-0.01
6CN	-1.07	0.174

IR Spectra

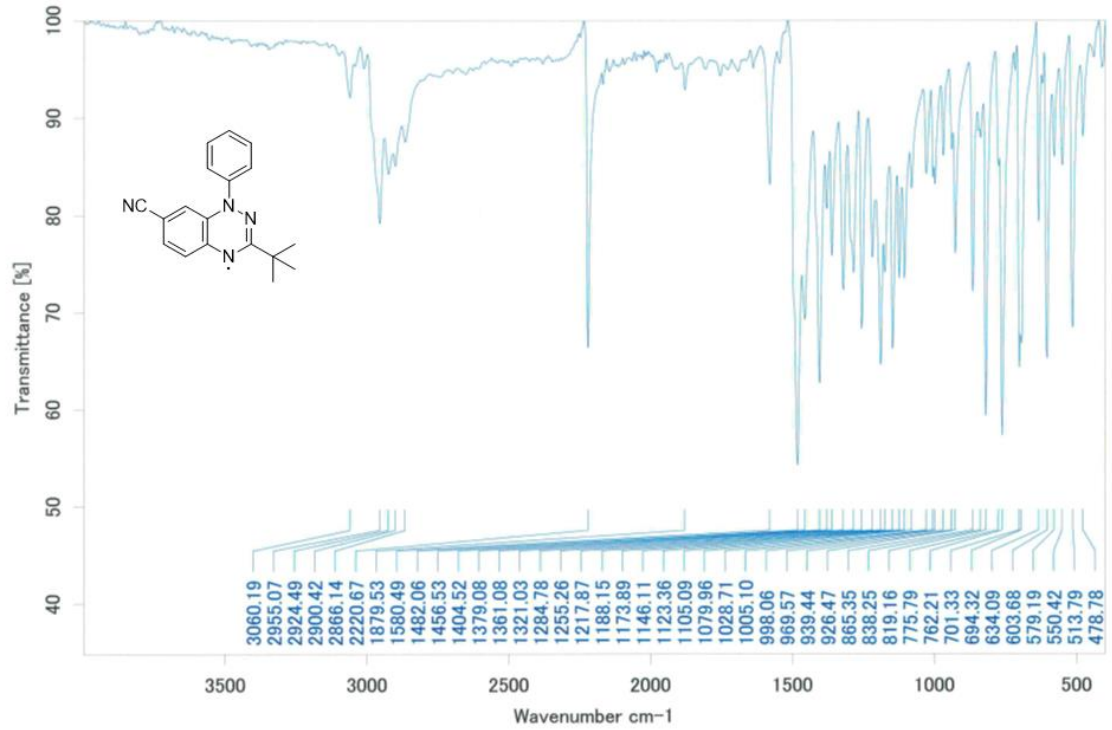
Transmittance [%]
100
90
80
70
60
50
40
NC
3060.19
2955.07
2924.49
2900.42
2866.14
2220.67
1879.53
1580.49
1482.06
1456.53
1404.52
1379.08
1361.08
1321.03
1284.78
1255.26
1217.87
1188.15
1173.89
1146.11
1123.36
1105.09
1079.96
1028.71
1005.10
998.06
969.57
939.44
926.47
865.35
838.25
819.16
775.79
762.21
701.33
694.32
634.09
603.68
579.19
550.42
513.79
478.78
3500
3000
2500
2000
1500
1000
500
Wavenumber cm−1

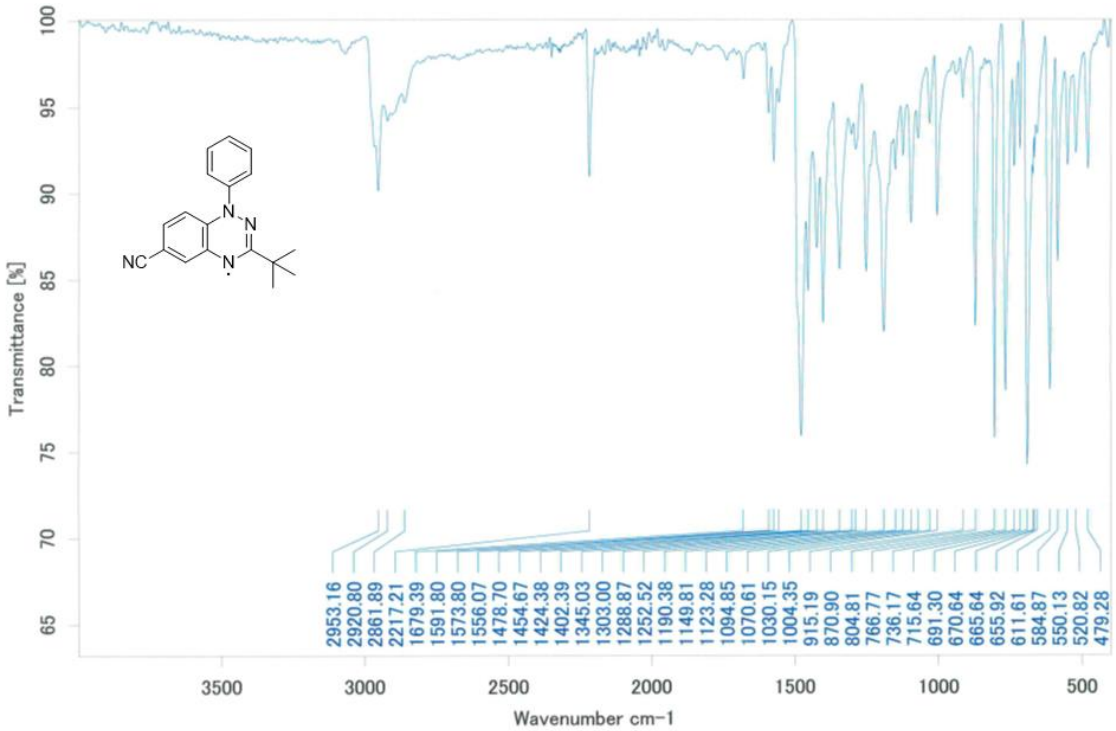
Transmittance [%]
100
95
90
85
80
75
70
65
NC
2953.16
2920.80
2861.89
2217.21
1679.39
1591.80
1573.80
1556.07
1478.70
1454.67
1424.38
1402.39
1345.03
1303.00
1288.87
1252.52
1190.38
1149.81
1123.28
1094.85
1070.61
1030.15
1004.35
915.19
870.90
804.81
766.77
736.17
715.64
691.30
670.64
665.64
655.92
611.61
584.87
550.13
520.82
479.28
3500
3000
2500
2000
1500
1000
500
Wavenumber cm−1